Electron Elimination As a Step Toward Long-Term Non-Neutral Ion Plasma Confinement

Chad Blaine Williams

A senior thesis submitted to the faculty of
Brigham Young University
in partial fulfillment of the requirements for the degree of

Bachelor of Science

Bryan G. Peterson, Advisor

Department of Physics and Astronomy

Brigham Young University

August 2011

ABSTRACT

Electron Elimination As a Step Toward Long-Term
Non-Neutral Ion Plasma Confinement

Chad Blaine Williams
Department of Physics and Astronomy
Bachelor of Science

In order to increase the confinement time of a non-neutral ^{7}Be ion plasma in a Malmberg-Penning trap we have implemented an electron dump system to expel electrons from the plasma. Ridding the plasma of electrons is important because it allows the ion plasma to respond correctly to the implemented rotating wall, which is designed to increase the ion central density and confinement time. The electron dump shifts the voltages on the plasma confinement rings to make them all negatively charged, thus forcing the electrons to leave. Theoretically, this can be accomplished without disrupting the ion plasma. We built an AC coupling box to coordinate the ring shifts and arranged the system to be run automatically through LABVIEW. After extensive tests of our system we have found that it decreases the electron density by a factor of 100, though issues, such as the disruption of the ion plasma, still remain.

Keywords: plasma, confinement, electron dump, ion, ^{7}Be

ACKNOWLEDGMENTS

First and foremost, I must thank Dr. Bryan Peterson for his longsuffering and patience, despite my ineptitude. His guidance, teaching, and confidence were central to my research and learning here at BYU. Also, I thank my wife, Leilani, for her support despite very late nights on campus. Lastly, I thank my parents for their unwavering support, even if they were not always exactly sure what I was working on, especially my father for piquing my interest in science almost two decades ago.

Contents

List of Figures

List of Tables

Chapter 1

Introduction

1.1 The Nature of ^{7}Be

Beryllium-7 is a common component of the atmosphere. It forms in spallation reactions when cosmic rays impact atoms, such as nitrogen and oxygen, in the upper atmosphere. These impacts cause the original atoms to be split into smaller pieces, some of which emerge as ^{7}Be atoms. Due to its universal distribution, ^{7}Be is a very useful tool in our quest to understand chemical, physical, and geologic procceses. For example, ^{7}Be, serves as a tracer element, which can be analyzed to understand the effects of cosmic rays on the atmosphere [1]. For example, high levels of ^{7}Be have been correlated with very low levels of solar activity while low levels of ^{7}Be have been correlated with high levels of solar acitivity, including the number of sun spots [2].

Additionally, ^{7}Be can be analyzed at the surface of the planet. Due to the possibility of ^{7}Be becoming attached to aerosols in the atmosphere, it may become deposited in surface sediment. Once deposited it can be used to trace the rates of soil erosion and deposition in a given area. If deposited in aqueous environments it has a tendency to attach to suspended particles, and can thus be used to determine the amount of sediment that is deposited and then resuspended in rivers and

lakes during the yearly flood cycle [3].

Beryllium-7 is also an important factor in solar neutrino astrophysics. Indeed, in the proton-proton chain that occurs in the sun, the decay of ^{7}Be by electron capture occurs in 15% of the total reactions. The neutrinos released by this reaction may have energies of nearly one MeV, which can be readily measured from Earth and used to better understand the nuclear reactions of the sun [4]. Beryllium-7 is also a terrestrial indicator of solar wind events [1]. Thus, a better understanding of the behavior and properties of ^{7}Be will allow us to understand many aspects of the natural world to a greater degree, including Earth's atmosphere, sediment deposition cycles, and solar astrophysics.

However, it is difficult to understand fully the behavior of ^{7}Be samples because its radioactive behavior and half-life are not well understood. Due to the small energy gap between ^{7}Be and ^{7}Li, ^{7}Be decays only through electron capture. Thus, its half-life is extremely dependent on its total number of electrons [5]. Voytas, et al. showed that, while ^{7}Be can decay by either capturing a 1s electron and then allowing a 2s electron to fall into the 1s state, or by direct capture of a 2s electron, the former decay will occur 96% of the time [6]. However, the total number of electrons, and thus the number of 2s electrons, remains important because it affects the effective electron number felt by the nucleus.

Typically, in order to measure the half-life of ^{7}Be, ^{7}Be is either formed into a compound or implanted in another material, such as gold, tantalum, aluminum, or aluminum oxide [7]. The problem with this method arises from the bonds that ^{7}Be forms with its surrounding atoms. These bonds force beryllium to share its outer electrons with its neighbors, thus changing its effective number of 2s electrons and affecting its half-life accordingly. For example, Das and Ray performed calculations using the tight-binding linear muffin-tin orbital method (TB-LMTO) that takes into consideration the electron affinity of various materials as well as their lattice geometry. They found that, for the examples above, ^{7}Be has 0.42, 0.60, 0.63, and 0.79 2s electrons on average respectively. Through comparisons with recorded experiments (see Table 1.1), Das and Ray found

that for the above examples, ^{7}Be has a measured half-life (in days) of 53.311, 53.195, 53.170, and 52.927 respectively [7]. Thus, they showed that the half-life can vary by as much as one percent in the lattices chosen. Figure 1.1 is the graph that they produced to show the dependence of the decay rate, which is inversely proportional to the half-life, on the number of 2s electrons. Table 1.1 contains the identification, measured half-lives, and references used by Das and Ray that correspond with the numbered data points in Figure 1.1.

However, since naturally occuring ^{7}Be in the atmosphere is involved in none of these compounds, we can only use this data to make inferences as to how it behaves in its elemental state. Thus, despite the abundance of ^{7}Be in the atmosphere, we do not completely understand its properties.

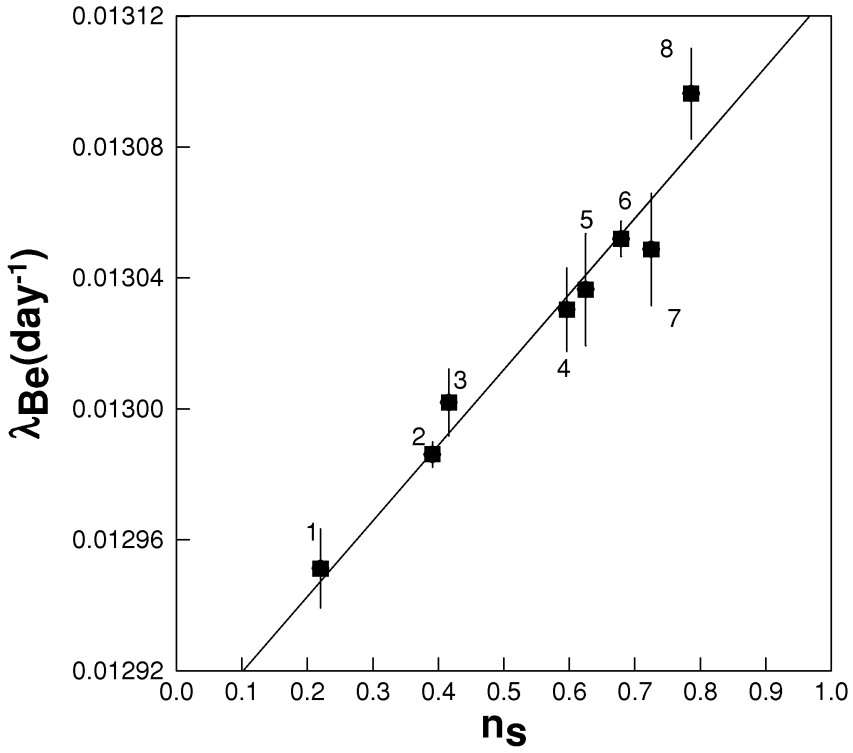

Figure 1.1 Dependence of decay rate of ^{7}Be on number of electrons in its 2s shell based on experimental and computational data. For data point references, refer to Table 1.1

Table 1.1 Correlation of numbered data points from Figure 1.1 with ^{7}Be compounds and measured half-lives

Number	Compound	Measured half-life in days	Reference
1	Average of BeO, BeF_2, and $Be(C_5H_5)_2$	53.520	[8]
2	Natural Beryllium	53.376	[9]
3	^{7}Be in Au	53.311	[10]
4	^{7}Be in Ta	53.195	[10]
5	^{7}Be in Al	53.170	[11]
6	^{7}Be in graphite	53.107	[10]
7	^{7}Be in LiF	53.120	[12]
8	^{7}Be in Al_2O_3	52.927	[13]

1.2 The Goal of Our Experiment

Our goal is to experimentally measure the half-life of ^{7}Be. In order to avoid the snags that have encumbered this measurement in the past, we plan to create a plasma of singly ionized ^{7}Be atoms in vacuum, thus dissuading them from bonding with other atoms. We also want to ensure that there are no free electrons present in the plasma in order to eliminate the possibility of recombination to form neutral atoms. This ionization will also ensure that all of the ^{7}Be will be found in the same state and we will know exactly how many electrons are associated with each atom, namely two 1s electrons and one 2s electron. We can be sure that no neutral ^{7}Be atoms will appear in the plasma because neutral atoms will not be confined by the magnetic and electric fields that will confine the ionized atoms. An important consequence of having all of the atoms in the same state is that they will all have the same decay rate, which we can then measure by utilizing the mass difference between ^{7}Be and ^{7}Li and the technique of Fourier Transform Ion Cyclotron Resonance Mass Spectrometry (FTICR/MS) to determine how many parent and daughter nuclei remain trapped after a given

period of time. In its singly ionized state $^7Be^+$ will decay to $^7Li^+$. Based on an extrapolation of Figure 1.1 we expect our results to yield a faster decay rate, and hence a shorter half-life, than those measured previously.

In order to successfully measure this half-life, we want to confine the plasma for one full half-life of ^{7}Be. To accomplish this, we have constructed a Malmberg-Penning trap.

1.3 The Malmberg-Penning Trap

The basis for our Malmberg-Penning trap is a large solenoid magnet that confines the plasma radially and end potential rings to provide axial confinement. Thus, the plasma is constrained to form a small rounded cylinder on axis between the end potentials. The trap is constructed of a series of concentric metal rings of varying lengths. On one end of the trap is a source, used to create the plasma, and on the other end is a set of charge collectors to collect the plasma at the end of its confinement time.

Our trap is constructed of copper rings of various lengths, but with a standard radius of 4 cm, as shown in Figure 1.2. Toward the source (to the right of Figure 1.2) are three longer rings of 5 cm each. Beginning with the ring closest to the source, these rings are called the Fill A (FA),

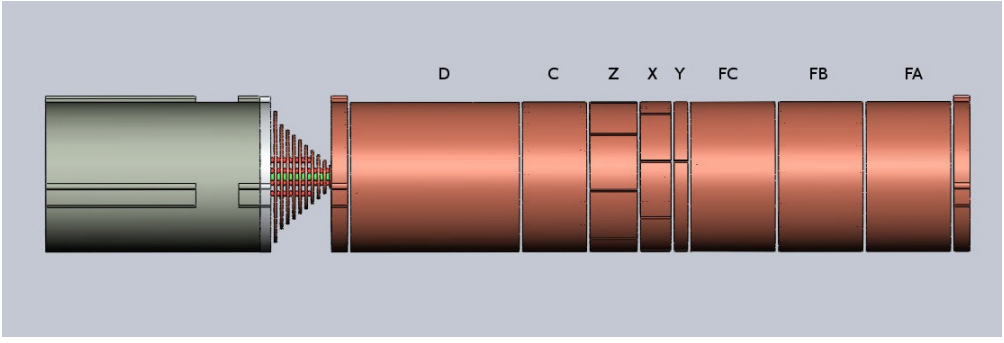

Figure 1.2 Diagram of Malmberg-Penning Trap ring structure. The source is found to the right of the picture.

Fill B (FB), and Fill C (FC) rings respectively, because they are used as a potential barrier to trap and compress the plasma during the initial fill sequence. This process of creating and trapping is also refered to as the stack. On the opposite side of the trap, towards the charge collectors, is the Dump Ring (D), which is 10 cm long. It too functions as a potential barrier to trap the plasma, and when its potential is lowered the plasma is allowed to flow out of the trap onto the charge collectors. We refer to this process as the dump. For the rest of this paper, these four rings (FA, FB, FC, and D) will be referred to as the end rings. In between the fill and dump rings are a set of axially shorter rings, labeled (from the fill end toward the dump end) as Y, X, Z, and C. The Y ring is 1 cm long and is segmented along its circumference into four sections. The X ring, which is 2 cm long, and the Z ring, which is 3 cm long, are each similarly divided into eight sections. The C ring is 4 cm long and is not segmented. However, throughout this paper, the X, Y, Z, and C rings will be referred to as the segmented rings. Each segment of each segmented ring and each of the end rings has a coaxial cable attached to it (not pictured) that allow us to either control or read the voltages induced on that piece during the operation of the trap. On either end of the rings are copper supports, through which we attach stainless steel threading which holds the ring assembly together, while behind the charge collectors is an additional aluminum support. We constructed the trap with small insulating glass beads between each segment so that none of the rings or individual ring segments are electrically connected to each other.

Our plasma source is a Metal Vapor Vacuum Arc, or MeVVA, source, shown in Figure 1.3. This consists of a small black disk of material contained in a holder to which we arc high voltages to create plasma. To initiate the stack sequence we lower the voltage of the entire housing to -150 V. We then continue to lower the potential of the cathode, which includes the inner piece of the housing and the source disk itself, toward -7000 V. The source is the black disk in Figure 1.3 and the the cathode is the large copper piece on the right. At some point before reaching -7000 V a breakdown occurs across the insulator between the anode and cathode and we get an

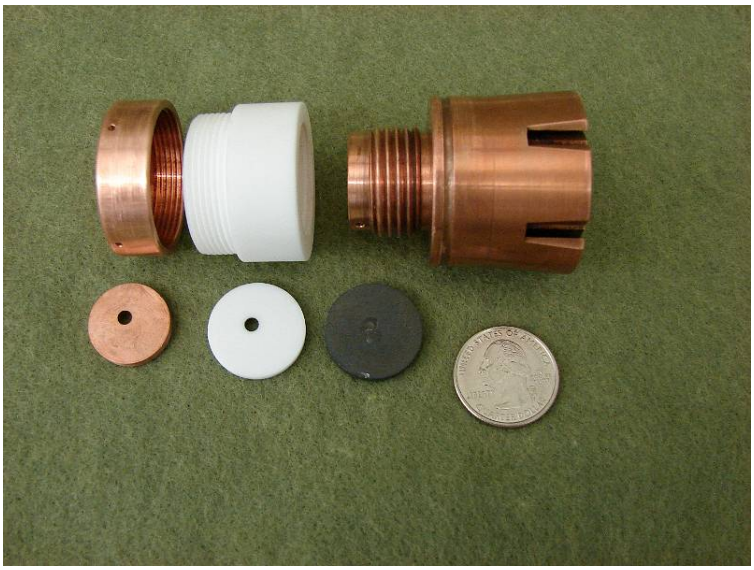

Figure 1.3 Split-away view of source holder. The black wafer is the source.

arc through a hole in the insulator. The anode is the small copper piece with a hole in it at the bottom of Figure 1.3, which the insulator is the white piece with a hole in it. The disk then ejects the ionized material which is propelled by a charged grid and guided by a smaller source magnet into the ring confinement area, at which point we raise the potentials of the end rings to trap the plasma. This ionized material is composed of both ions and electrons which create, in effect, two separate plasmas — one composed of entirely ions and the other of electrons.

At this time, for cost and simplicity we are using disks of boron carbide. When we are confident that our machine is functioning properly we will create disks of enriched ^{7}Be in our Van de Graaf accelerator by bombardment of enriched ^{10}B with protons to produce alpha particles and ^{7}Be according to the equation:

$$ {}^{1}_{1}\mathrm{p} + {}^{10}_{5}\mathrm{B} \rightarrow {}^{4}_{2}\mathrm{He} + {}^{7}_{4}\mathrm{Be} \tag{1.1} $$

The charge collectors consist of ten concentric copper disks of increasing radius with the smallest disk closest to the D ring and the largest disk farthest from it, as shown in Figure 1.4. When

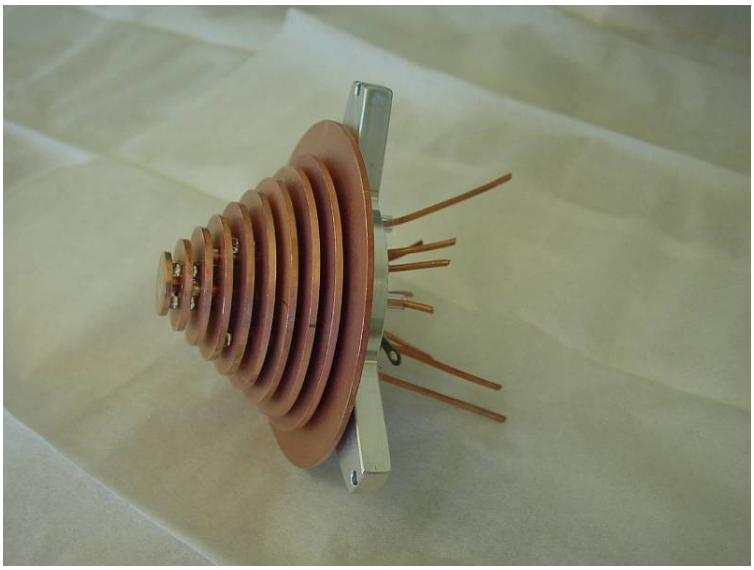

Figure 1.4 Side view of the charge collectors showing the differing diameters of the disks. The left end of this picture is closest to the D ring.

the plasma is dumped after the chosen confinement time, the potential of the D ring drops to zero and the plasma follows the magnetic fields lines parallel to the axis of the trap directly to the disk at its corresponding radius. The change in charge on each disk is then integrated and sent to the computer via LABVIEW. From this data we can reconstruct the density profile of the plasma that was present in the machine at the time of dumping.

Chapter 2

Electron Elimination

2.1 Problems with Long-Term Confinement

Due to the presence of an axial magnetic field in the Malmberg-Penning trap, both the ion and electron plasmas are radially confined by cyclotron motion. However, in practice we find that over time dispersive forces overcome the centripetal force of cyclotron motion. The first source of dispersion is irregularities in the fields, especially in the magnetic field. Even though we have added correction coils to our solenoid, such irregularities will always exist. The other cause of dispersion is residual neutral atoms. Even at a pressure on the order of 10^{-9} torr there are sufficient collisions to disperse the plasma. Due to the strong positive electric field caused by the ion plasma, any collisions with neutrals will force the ions to move outward, down the potential gradient. Over time, the plasma can be pushed to the wall and disperse. There also exists the possibility that ion and electron plasmas can partially recombine to create neutral atoms which cannot be trapped in magnetic and electric fields. Due to these reasons, we find that within only a few minutes of trapping that very little plasma is left in the trap.

2.2 The Rotating Wall

In order to recompress the plasma, we have implemented a rotating wall system similar to that developed by X.-P. Huang, et al. at the University of California, San Diego [14]. In this system, sinusoidal AC voltage waveforms are applied to the segments of the X ring. Identical to the system set up by Huang, the eight wall segments have voltages V_j, where $j = 1...8$, with phases spaced out in increments of $\frac{\pi}{4}$, given by $\theta_j = \frac{2\pi j}{8}$. The voltage on each segment is then given by $V_j = A\cos\left(\theta_j - \omega_{RW}t\right)$, where A is the amplitude of the signal and ω_{RW} is the rotating wall angular frequency [14]. For example, the waveform applied to the first segment (XA) has a phase of 45°, the segment XB has a phase of 90°, and so forth to create a dipole field around the plasma. We typically use an amplitude near 2 V, though the exact value has been shown to be of little importance [15].

This dipole field causes a radial bulge in the plasma, so that its cross-section resembles an ellipse more than a circle. As the field rotates, it couples with the plasma and drags the plasma bulge with it. This applied torque increases the angular momentum of the plasma. It has been found that if ω_{RW} is greater than the $E \times B$ rotation frequency of the plasma (ω_E) then the rotating wall will cause the plasma to rotate more quickly and compress, while if ω_{RW} is less than ω_E then the plasma will rotate more slowly and expand. Thus, while the rotating wall is applied, the central density, n, will slowly change until ω_E equals ω_{RW} [15]. In our case, this means that n will slowly increase. The plasma will move radially toward the center of the trap instead of dispersing, allowing us to confine the plasma for much longer periods of time. By using this technique, Huang, et al. found that they could maintain their plasma indefinitely with central densities as high as $10^7\,\mathrm{cm}^{-3}$, or 20% of the Brillouin limit [14].

However, experimentally we have seen that with both ion and electron plasmas present in the trap this system does not function correctly. After trapping the combined ion and electron plasma, we set the potential of the FB, FC, and D rings to 70 V and the potential of the X, Y, Z, and C

rings to ground. The ions are located under the grounded rings and have a space charge potential of approximately 30 V. Typically, the electrons are more attracted to the end potentials and the electron plasma forms two columns underneath either end potential. However, when the electron plasma has a high enough temperature the electrons can pass through the area occupied by the ions. This tends to partially or completely cancel out the ion potential and create a nearly neutral fluid in that region. Experimentally, this fluid responds incorrectly to the voltages applied by the rotating wall. The electron plasma reduces the effective electric field felt by the ion plasma which in turn reduces the $E \times B$ rotation frequency of the plasma, causing the ion plasma to expand instead of compress. Also, if the ions and electrons recombine then the effects of the end ring potential barriers and solenoid magnetic field are voided and the neutral atoms escape from the trap.

Hence, in order to maintain the plasma for the significant period of time required to measure the half-life of ^{7}Be we must first eliminate the electron plasma while maintaining the ion plasma.

2.3 Electron Dump: Procedure

We have tried various methods of electron elimination, including high-frequency voltage sweeps to excite the electrons without disturbing the ions and a pumping procedure to force them past the end rings. However, none of these ideas yielded much success. Recently, based on a discussion with Fred Driscoll of UCSD of his unpublished laboratory techniques, we have implemented a procedure to shift the confinement ring potentials so that the electrons feel only negative potentials on the rings, thus forcing the electrons to exit the trap. We call the procedure the electron dump.

Initially upon trapping the plasma, the end rings are maintained at 150 V while the segmented rings are held at ground as shown in Figure 2.1. The FA ring is turned off immediately upon trapping the plasma and remains off throughout the duration of the experiment. Hence, it is not included in the following discussion or figures.

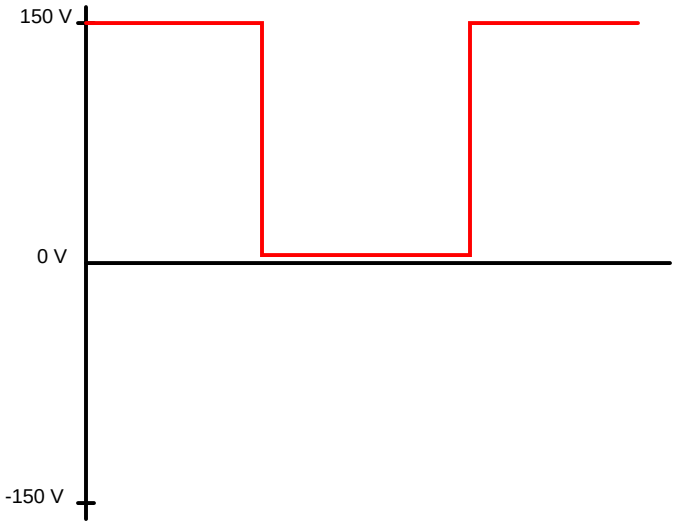

Figure 2.1 Initial Ring Configuration. The end rings are at 150 V and the segmented rings are at ground.

This 150 V potential barrier is extremely important for the confinement of the ions, some of which are very energetic after trapping. In order to block the ions from exiting while the electrons are being dumped, the segmented rings, under which we believe that the ions are confined, are first dropped to increase the potential barrier. During our initial tests we discovered that a sudden change of potential disrupts the plasma and causes it to disperse more quickly. Thus, in order to drop these rings we programmed LABVIEW[1] to execute a controlled drop of the rings. This drop must be done at a rate slower than the bounce frequency of the particles between the end potentials in order to not disrupt the plasma.

In order to control the drop we have programmed a LABVIEW VI to write several signals to the amplifiers that are connected to the various rings of the machine. To drop the segmented rings, LABVIEW writes one half of a sine wave that has been offset so that it grows monotonically from

[1]For block diagrams of the LABVIEW VIs, see Appendix A

0 V to 5 V. This signal is then passed to a high voltage operational amplifier, which both inverts the signal and mutiplies it by a gain of 30, producing a slowly falling signal that drops from 0 V to −150 V over a period of 100 ms and then holds the rings at that potential. The entire process is depicted in Figure 2.2, plotted in terms of arbitrary time units, which shows the sinusoidal drop, constant voltage at the bottom, and then the the sinusoidal rise. We also added 300 H of inductance in series with the amplified signal to round off the transition edges even more. During this process, the end rings are maintained at 150 V, creating the potentials seen in Figure 2.3.

After the segmented rings have dropped we wait 70 ms before executing a similar process in

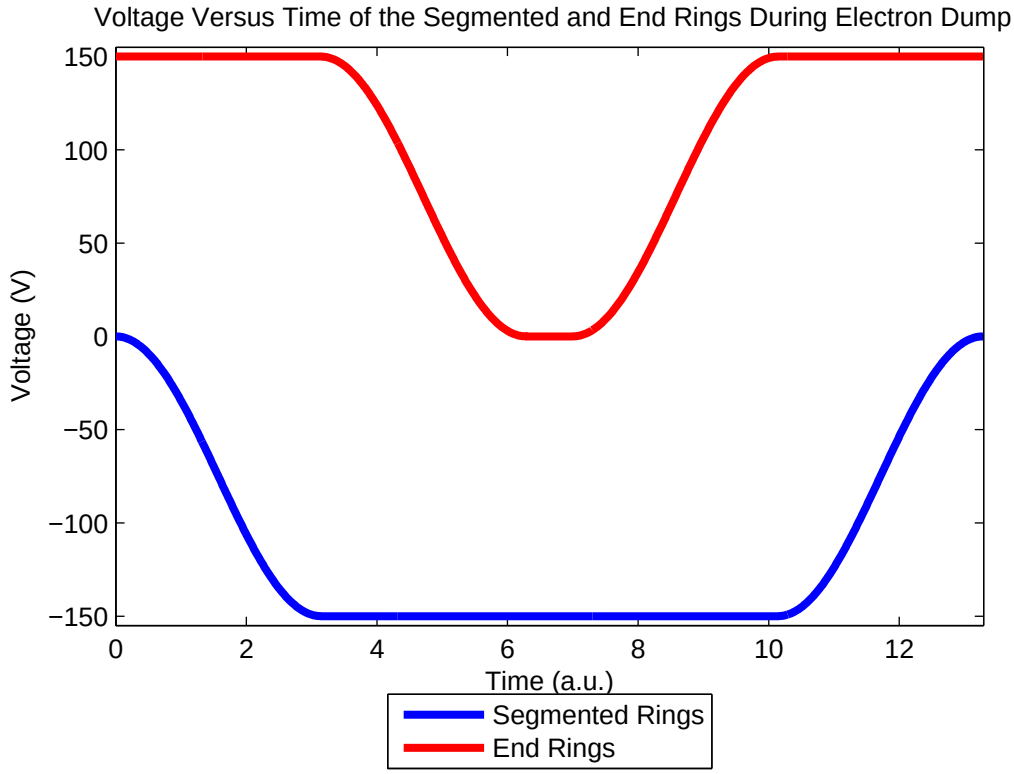

Figure 2.2 Plot of the segmented ring voltage versus time. This is the signal output by LABVIEW after it has gone through an amplifier with gain of −30. The drop of the end rings occurs during the time when the segmented rings are sitting at −150 V.

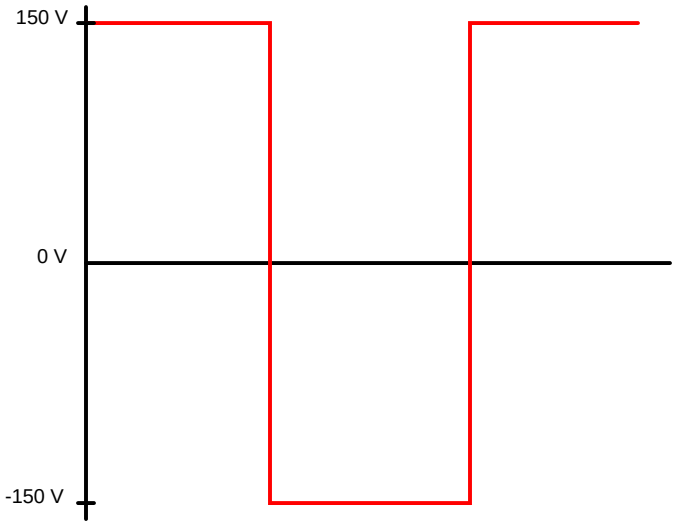

Figure 2.3 Middle Ring Configuration. The end rings are at 150 V while the segmented rings are at −150 V.

which LABVIEW gradually decreases the potential of the end rings until they are turned off, at which point they settle at a few volts below ground. With the entire trap thus negatively charged as shown in Figure 2.4, the electrons are repelled and are forced to leave through the ends of the trap. Once we have held the rings at these voltages for 100 ms, we first raise the end rings, recreating the potentials of Figure 2.3. After another 70 ms, we raise the segmented rings using the exact opposite of the function used to drop the potential, writing another half sine wave that this time returns from −150 V to ground. After this process, the ions are still trapped underneath the segmented rings, but there are no electrons left in the system.

2.4 Electron Dump: Circuitry

Unlike the larger end rings, the X, Y, Z, and C rings are not used to confine the plasmas. Instead we use them to control and read our diagnostics, such as the rotating wall and the FTICR/MS. Hence, during typical operation of the trap these rings must be connected to interfacing devices on

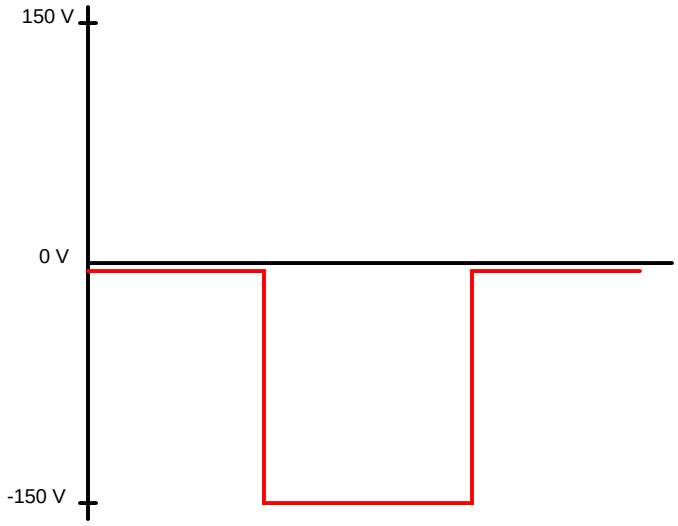

Figure 2.4 Dropped Ring Configuration. The end rings are at ground and the segmented rings are at $-150\,\mathrm{V}$.

the computer which communicate with LABVIEW. The X, Y, and Z rings read raw voltages and are thus connected to analog input boards on the computer. Since the C ring is used to calculate the total amount of charge loaded into the trap during the timed stacking process, it must connect to the computer through an integrator circuit.

However, in order for the electron dump procedure to function we must be able to connect the X, Y, Z, and C rings to $-150\,\mathrm{V}$. The computer cannot be used for this task because its output is limited to $5\,\mathrm{V}$. Thus, the rings must be connected to an alternate power supply in order to drop. The idea of the AC coupling box that we constructed is to connect each segment of these rings to a relay which can then connect to either the high voltage operational amplifier controlled by the computer or the computer interfacing devices. The AC coupling box nominally consists of a relay, a transistor to control current across the relay, and blocking capacitors to protect the computer and other equipment from high voltages.

For the X, Y, and Z rings the circuitry consists of a single relay that connects all segments of those rings to either ground or to the amplifier. After the plasma fill, a $5\,\mathrm{V}$ control voltage from

the computer connects to the base of an NPN transistor which allows current to flow through the relay. The relay switches from the normally closed state that connects the rings to ground to the normally open state which connects the rings to the amplifier. The computer, through LABVIEW, then drops the rings, waits, and raises them again. At the conclusion of the process, the computer switches off the control signal and the relay returns to the normally closed state so that the X, Y, and Z rings are grounded and can be controlled by the computer. The circuit diagram for this AC Coupling box is found in Figure 2.5. The blocking capacitor between the input and outputs of each segment of these rings ensures that the $-150\,\mathrm{V}$ signal never connects to the computer, while the $1.0\,\mathrm{M\Omega}$ resistor protects the components from high currents and isolates the connectors for each segment from each other.

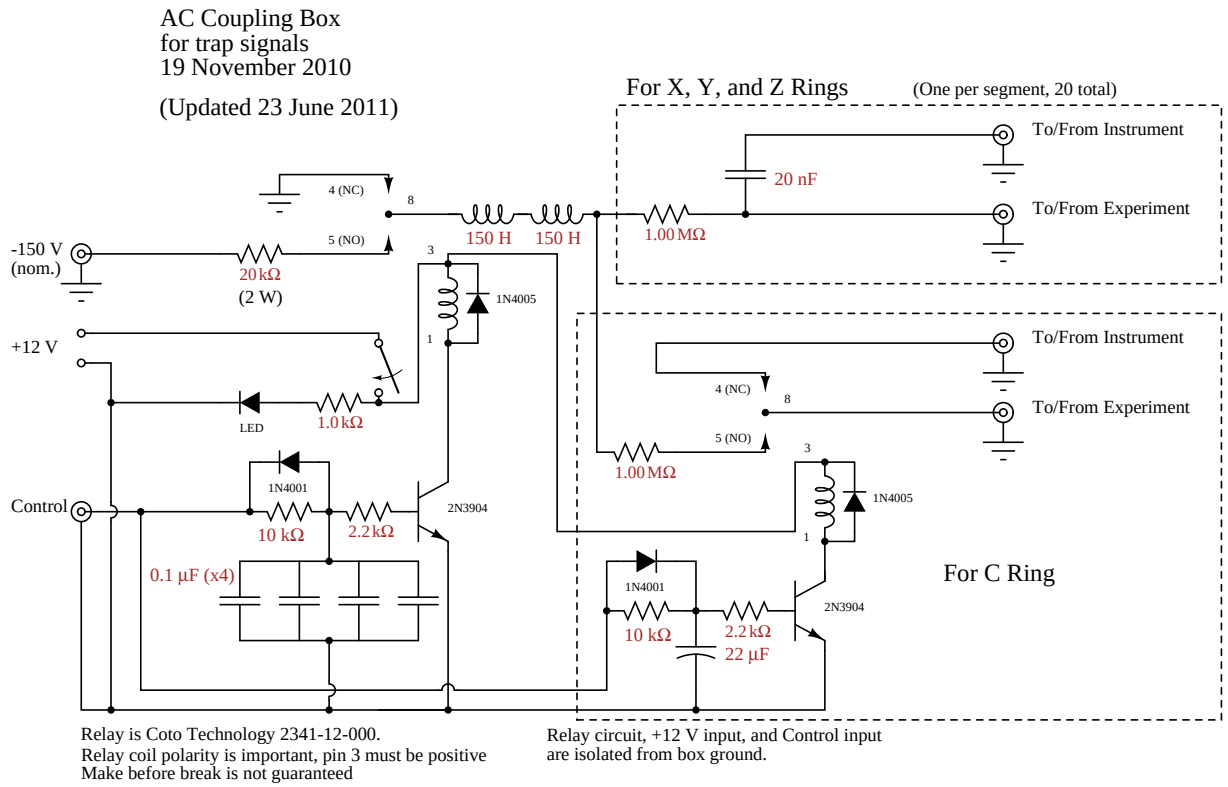

Figure 2.5 A schematic showing the circuitry of the AC coupling box

Since the C ring connects to the computer through an integrator, its circuitry is more complicated. First of all, we found experimentally that a blocking capacitor similar to the one used on the other rings interferes with the operation of the integrator, so we replaced it with an extra relay to protect the op-amp of the integrator from $-150\,\mathrm{V}$. Secondly, we inserted some timing circuitry because neither break-before-make nor make-before-break can be guaranteed with the relays that we used. Thus, we cannot guarantee that the $-150\,\mathrm{V}$ from the amplifier will never contact the sensitive circuitry of the integrator unless it is timed correctly.

The normally closed state of the additional C relay is to connect the C ring to the integrator, whereas the normally open state is to connect the C ring to the output of the main relay — either ground or the amplifier. The order of the switching of these relays is very important. The C relay must switch off of the the integrator before the main relay switches to the amplifier so that the integrator never connects to the high voltages of the amplifier. After the dropping and raising process is complete, the C relay must wait for the main relay to switch back to ground before reconnecting with the integrator. The extra $10\,\mathrm{k}\Omega$ resistor, capacitors, and 1N4001 diode attached to the base of the transistors in Figure 2.4 insure that this sequence is followed. The diode with its cathode toward the base of the transistor allows the relay for the C ring to switch quickly when the control voltage is initially turned on, while the diode on the main relay delays the switch of the relay. Hence, the integrators disconnect first. Once the control voltage is turned off, the diode on the main relay with its anode toward the base of the transistor allows its attached capacitors discharges faster than those connected to the diode on the C relay, allowing the main relay to connect to ground before the integrators are reconnected to the C ring. Thus, through careful timing we allow the C ring to drop to $-150\,\mathrm{V}$ while protecting the integrator circuit.

Chapter 3

Results and Discussion

3.1 Measuring the Results

In order to determine the total number of electrons and ions present in the trap, the voltages collected by the charge collectors at the end of each run are saved by the computer. We then use a MATLAB program that performs a least-squares fit to analyze the data points and calculate the respective central densities and particle number totals for the separate ion and electron plasmas. This program also prints a graph that allows us to see the plasma profile. Ideally, such a figure would look like Figure 3.1, which was taken at the beginning of May, 2011 and was one of the earlier test runs of the electron dump. This plot graphs the line integrated density of the plasma versus the effective radius. A positive density indicates the presence of a mostly ion plasma, while a negative density indicates the presence of an electron plasma. From experimentation, we expect to see the line integrated density to reach from the order of 10^9 to $10^{11}\,\mathrm{m}^{-3}$ at a zero effective radius. For our trap, given the strength of our magnetic field, we expect the Brillouin limit to be $1.7 \times 10^{13}\,\mathrm{m}^{-3}$. Experimentally we have seen that random noise in the trap corresponds to density values on the order of $10^8\,\mathrm{m}^{-3}$.

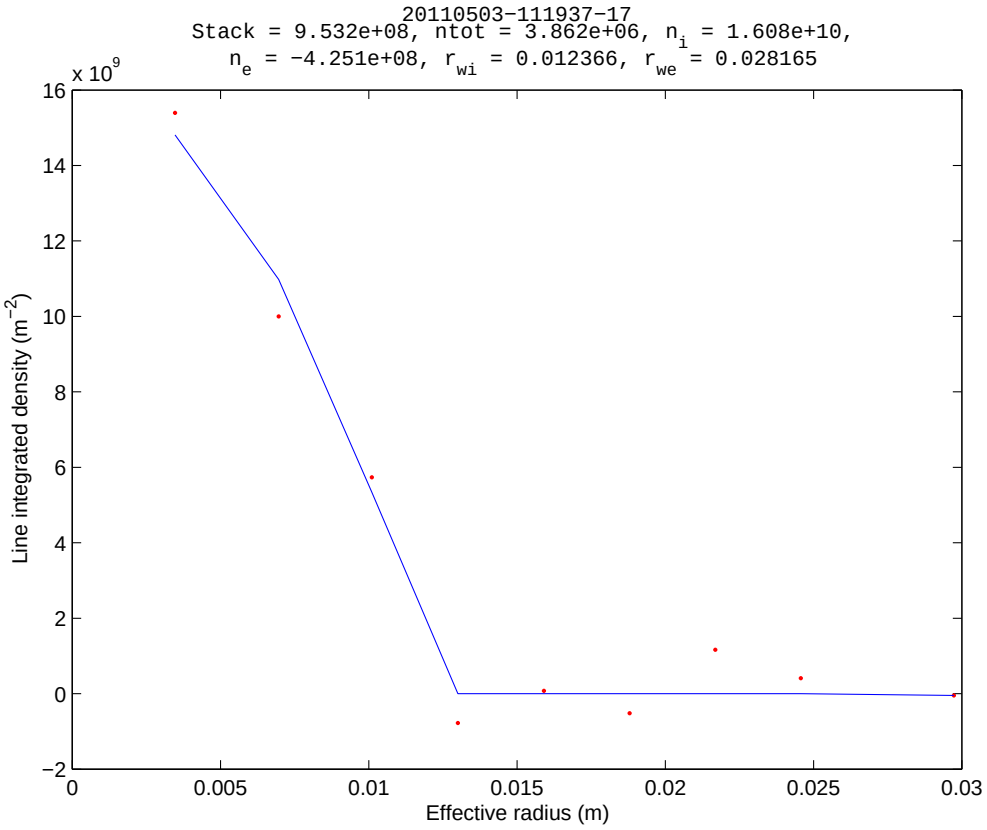

Figure 3.1 Ideal density versus radius plot for an ion plasma. Note the positive ion concentration in the middle that drops abruptly to zero at larger radii

Figure 3.1 clearly shows the expected behavior of a purely ion plasma. It has a relatively high postive line integrated density near the center that drops quickly to zero at 1.2 cm and remains at zero out to the edge of the plasma. This particular plasma contains an ion central density of $n_i = 1.6 \times 10^{10}\,\mathrm{m}^{-3}$ while its electron central density is computed to be $n_e = -4.2 \times 10^{8}\,\mathrm{m}^{-3}$, which we interpret as a calculational remnant of the computer trying to force a fit to a nonexistent parameter. We thus interpret such values as zero, or at least very small compared to n_i. In this way we obtained all of our data points for comparison.

3.2 Results

After our initial tests it appeared that the electron dump was successfully removing the electron plasma without disrupting the ion plasma, as explained in Section 3.1. However, due to apparent inconsistencies in the stacking data we took time to analyze other procedures that were happening in our system. Unfortunately, we realized that we had made errors in timing which affected the stack. After fixing these errors we found that the electron dump was unexpectedly eliminating both ions and electrons, despite the fact that the changes we made were unrelated to the electron dump or to the plasma dump. This ion loss became apparent by looking at the density plots for the various cases. A plot for the case in which the electron dump does not occur is seen in Figure 3.2. Here we see that the whole plot has a negative density, indicating an overwhelming presence of electrons, though there is a bump in the middle where the graph is less negative, indicating the presence of ions. Both an electron plasma and an ion plasma are clearly visible in the graph. However, when the electron dump is turned on, we now typically collect data that more closely resembles Figure 3.3. The data points are arranged nearly randomly and, most importantly, the central density is low enough to consist of just noise. In order to reduce this disruption we have tried various methods, including lowering the segmented rings and the end rings simultaneously so as to maintain the potential difference between the two sets of rings at 150 V throughout the entire procedure. However, we found no marked improvement. The data taken for the following analysis was taken after these changes were made.

To test the electron dump we took hundreds of samples with varying parameters. For this particular analysis, we took fifty samples — twenty-five with the electron dump turned on, and twenty-five with the electron dump turned off. These samples were taken after whatever change occured so they show decreased densities of both ions and electrons. We found that without the electron dump turned on, the electron central density had a value of $n_e = 1.72 \times 10^{12}\,\mathrm{m}^{-3}$. When the electron dump is switched on, however, $n_e = 5.72 \times 10^{9}\,\mathrm{m}^{-3}$. These numbers exclude any

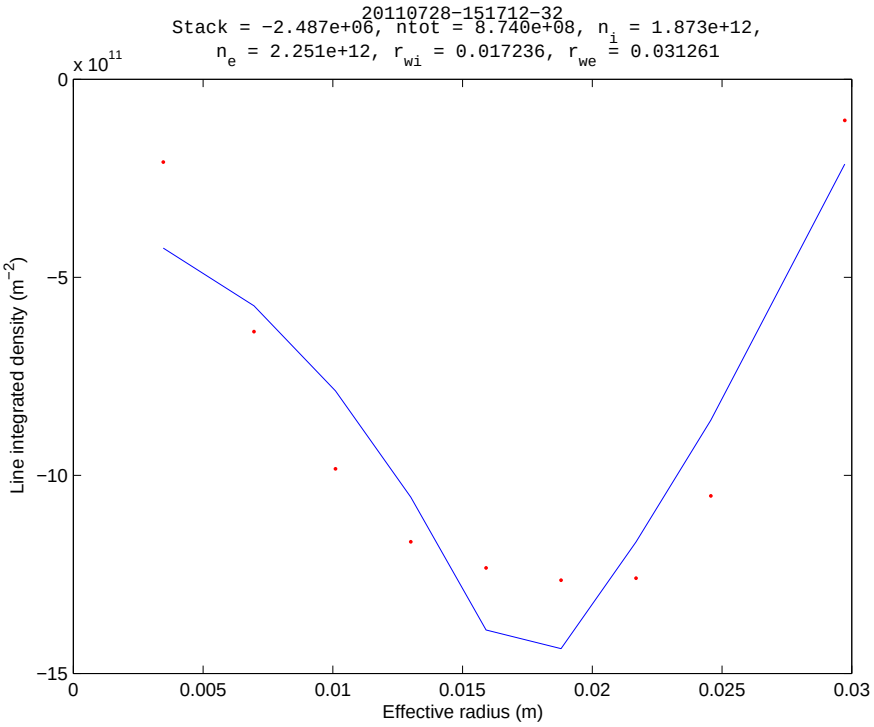

Figure 3.2 Line-integrated density plot for the plasma when the electron dump is turned off. Notice the less negative bump in the middle that indicates ions as well as the overall prevalence of negative charge.

erratic values that indicate that no plasma was present, as discussed in section 3.1.

In order to more accurately compare these values, we scaled them by the ratio of the average stacking values for each case. This is to eliminate the bias that arises from inconsistent stacking values. We expect that a higher stacking value should yield a higher particle total at the end of a run. We want to correct for this difference so that we can be sure that the experimental difference in n_e is due only to the electron dump. For the case in which the electron dump is off, the average stack was 1.21×10^7 particles whereas the average stack when the electron dump was on was 4.62×10^6 particles. The scale factor used for $\text{Stack}_{\text{off}}$ over Stack_{on} was then 2.63. This is because the stacks with the electron dump off were taken before those with the electron dump on and the source has a tendency to become less effective over the course of a day. After scaling, we

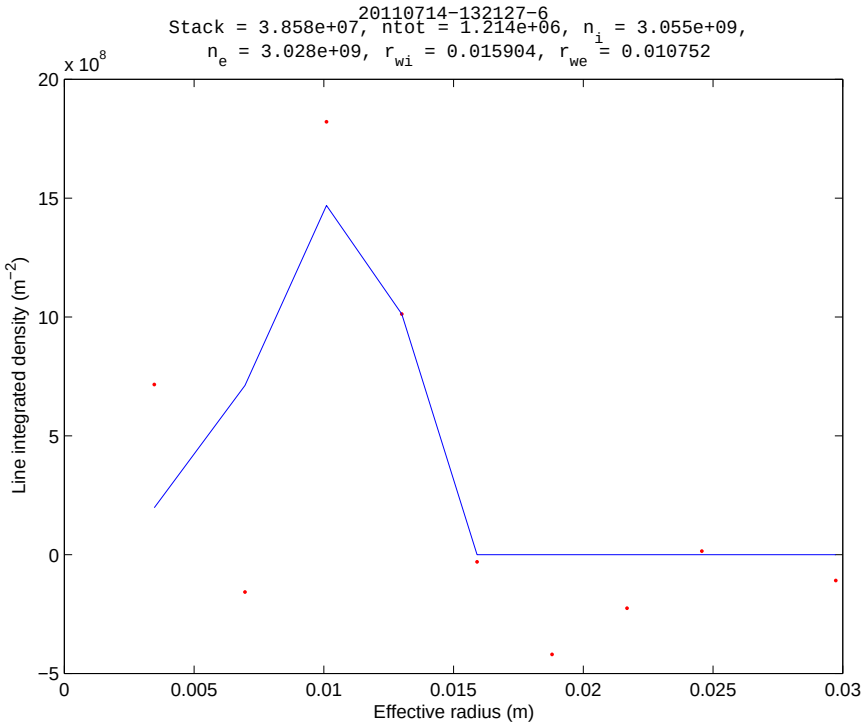

Figure 3.3 Line-integrated density plot for the plasma when the electron dump is turned on. Notice the low central density and seemingly random data points

found the ratio of n_e with the electron dump off to n_e with the electron dump on to be 114. Thus, the electron dump procedure effectively decreases the amount of electrons present by two orders of magnitude. This brings n_e down to noise levels, so we cannot be certain how far beyond the factor of 100 we have gone because we have reached the limits of our measurements. We have possibly decreased n_e by more than the measured value. Either way, with n_e at noise levels the ion plasma should behave as if no electron plasma is present.

3.3 Discussion

From its outset, the electron dump has had two main objectives. The first is to effectively eliminate the electron plasma and the second is to do so without disrupting the ion plamsa. Thus, up to this point it has fulfilled one of its objectives. With the electron density diminished by a factor of 100 we can trap and mantain idealized plasma such as that in Figure 3.1. Also, with such an electron decrease the ions will behave much more predictably to the effects of the rotating wall and we can overcome the effects of dispersion and confine the plasma for much longer periods. Before the sudden change in ion confinement we were able to maitnain our ion plasma for up to thirty minutes. This is certainly a step toward long-term confinement.

However, in order to achieve this, we must discover why the ions are being removed from the plasma in the first place. At some point during the past several months something happened that resulted in the elimination of the ion plasma as well. Whether its loss is a direct result of the electron dump or can be contributed to other factors we do not know at present. Thus, our current and future research will be dedicated to ascertaining the means and motive of the ion elimination so that those factors can be eliminated and we can maintain the ion plasma. In order to accurately measure the half-life of ^{7}Be we need to be able to consistently produce plasma similar to that shown in Figure 3.1. Thus, in order to accomplish the goal of our experiment we must be sure that the electron dump is working correctly. Then we must discover and fix our current our elimination problem.

Appendix A

LABVIEW VIs

This appendix contains all of the LABVIEW VI's that I personally wrote to control the electron dump, beginning with the highest level and progressing through its subVI's. The top-level VI to run the whole experiment, Testing.vi is not included.

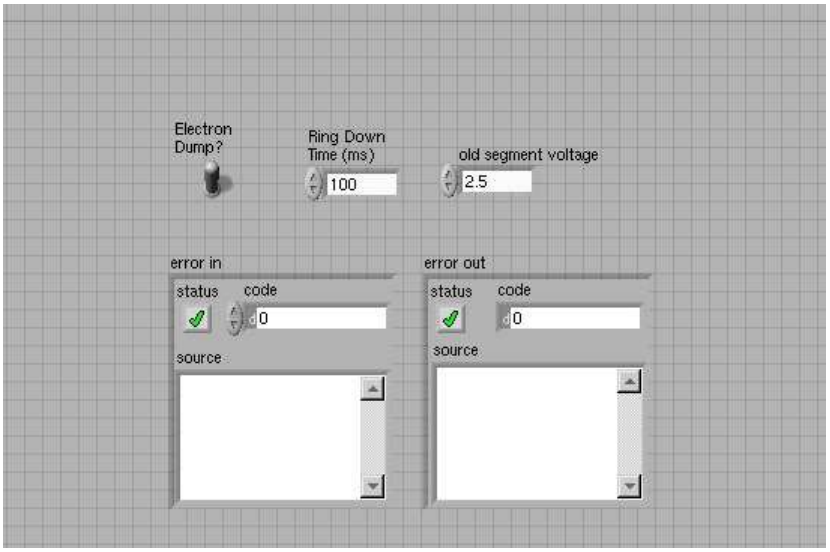

Figure A.1 Front Panel for DumpElectrons.vi, the top-level VI for the Electron Dump. This VI calls a subVI to drop the rings, waits for a predetermined period of time, and then calls another subVI to raise the rings.

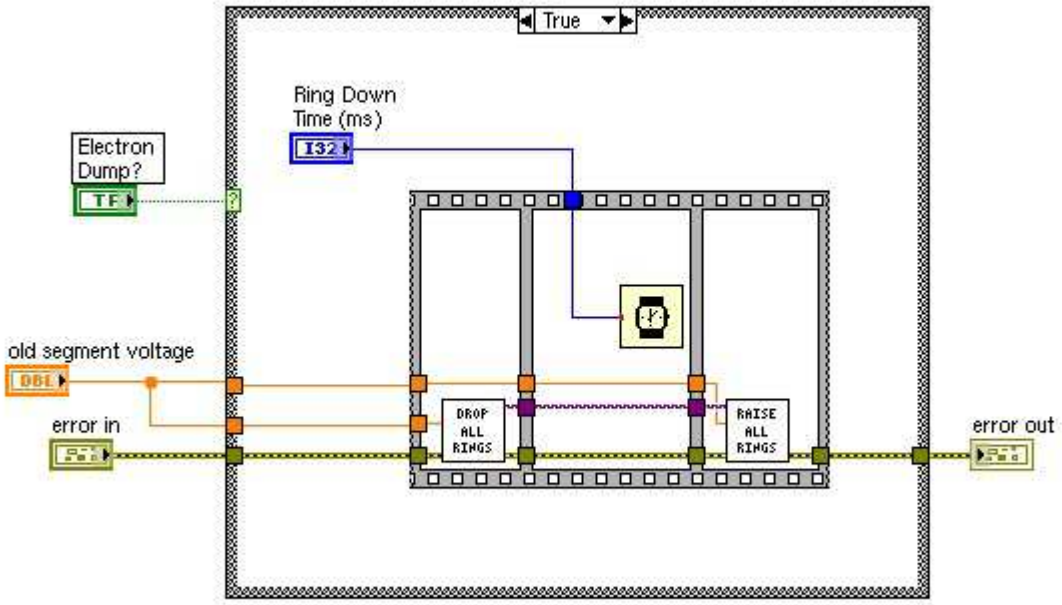

Figure A.2 Block Diagram for DumpElectrons.vi, the top level VI for the Electron Dump. The subVI "Drop All Rings" is seen in Figure A.3 and the subVI "Raise All Rings" is seen in Figure A.5

Figure A.3 Front Panel for Drop Rings.vi. This VI initiates a control voltage that switches the relay to connect the segmented rings to the op-amp. After it calls the subVI Drop Seg Rings.vi to drop the segmented rings (see Figure A.7) it controls the drop of the confinement rings.

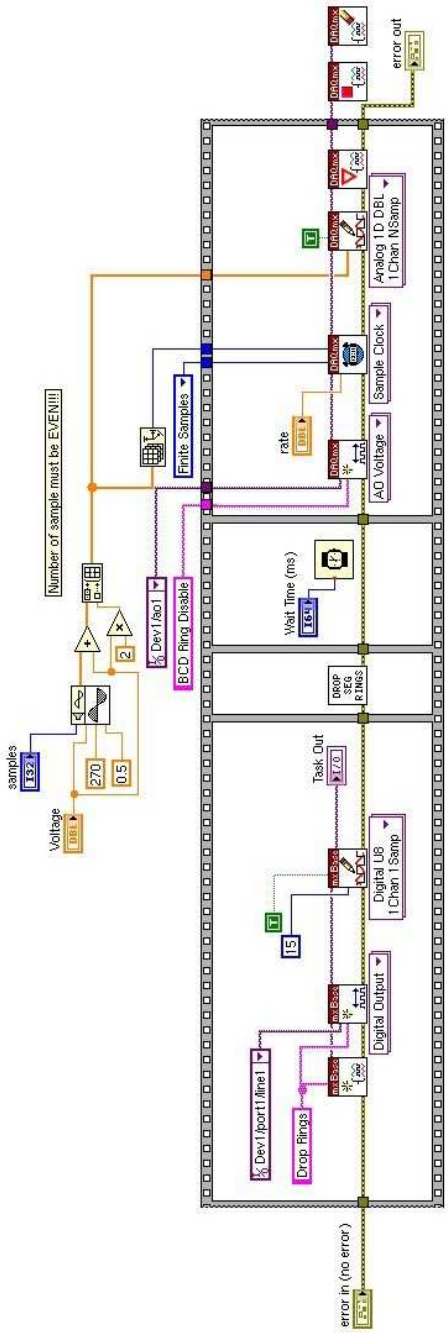

Figure A.4 Block Diagram for Drop Rings.vi. This VI initiates a control voltage that switches the relay to connect the segmented rings to the op-amp. After it calls the subVI Drop Seg Rings.vi to drop the segmented rings (see Figure A.7) it controls the drop of the confinement rings.

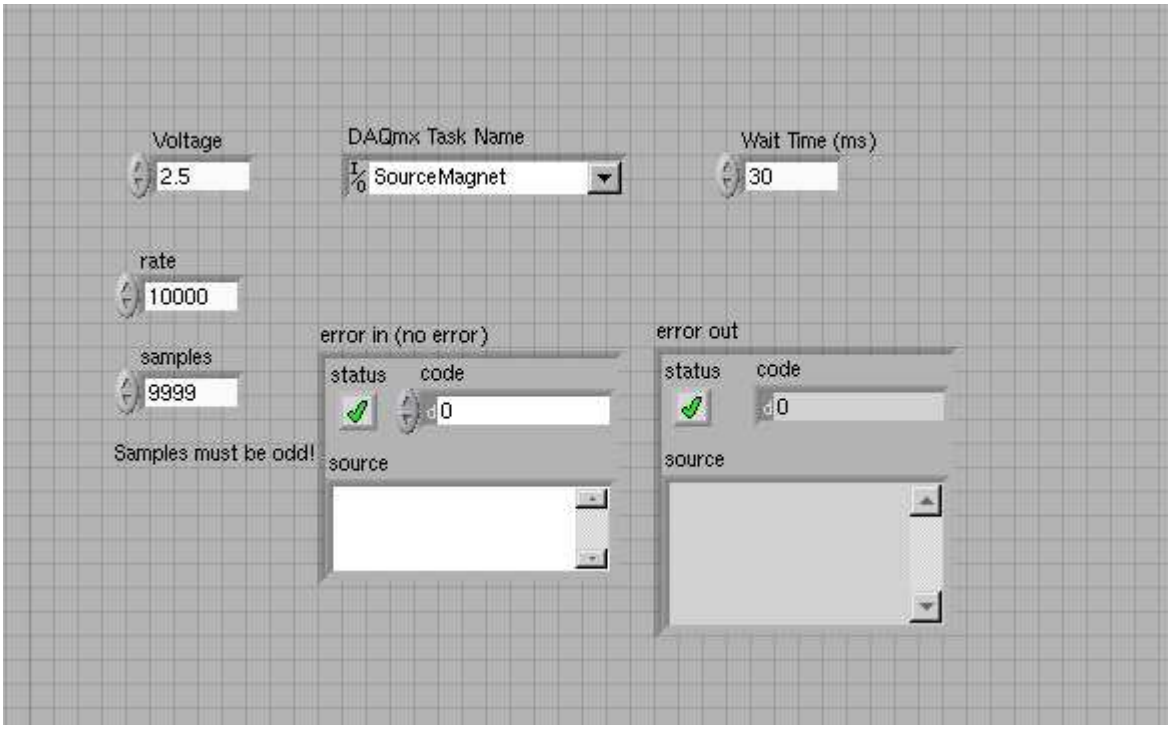

Figure A.5 Front Panel for Enable Rings.vi. This VI raises the confinement rings, then calls the subVI Raise Seg Rings.vi to raise the segmented rings (see Figure A.9), and finally shuts off the control voltage to the relay so that the segmented rings connect back to the computer.

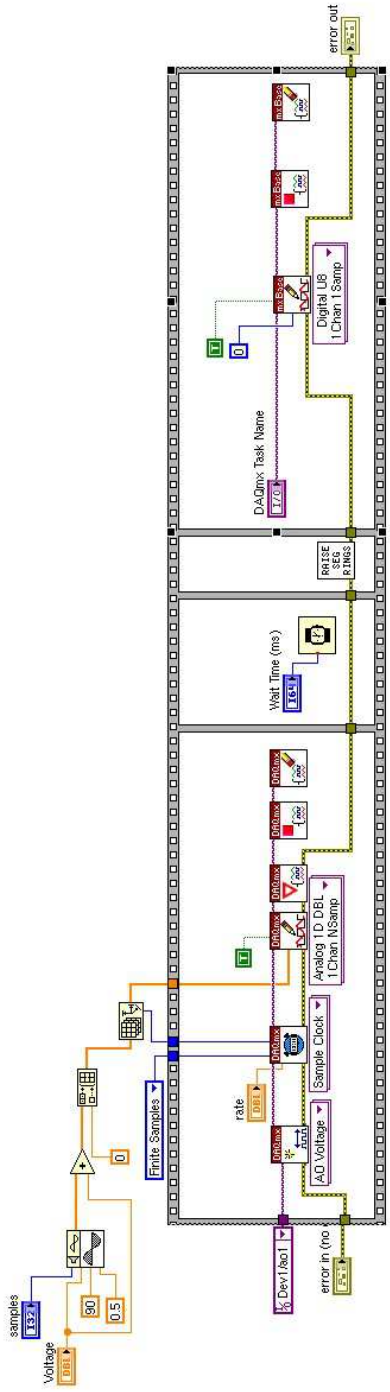

Figure A.6 Block Diagram for Enable Rings.vi. This VI raises the confinement rings, then calls the subVI Raise Seg Rings.vi to raise the segmented rings (see Figure A.9), and finally shuts off the control voltage to the relay so that the segmented rings connect back to the computer.

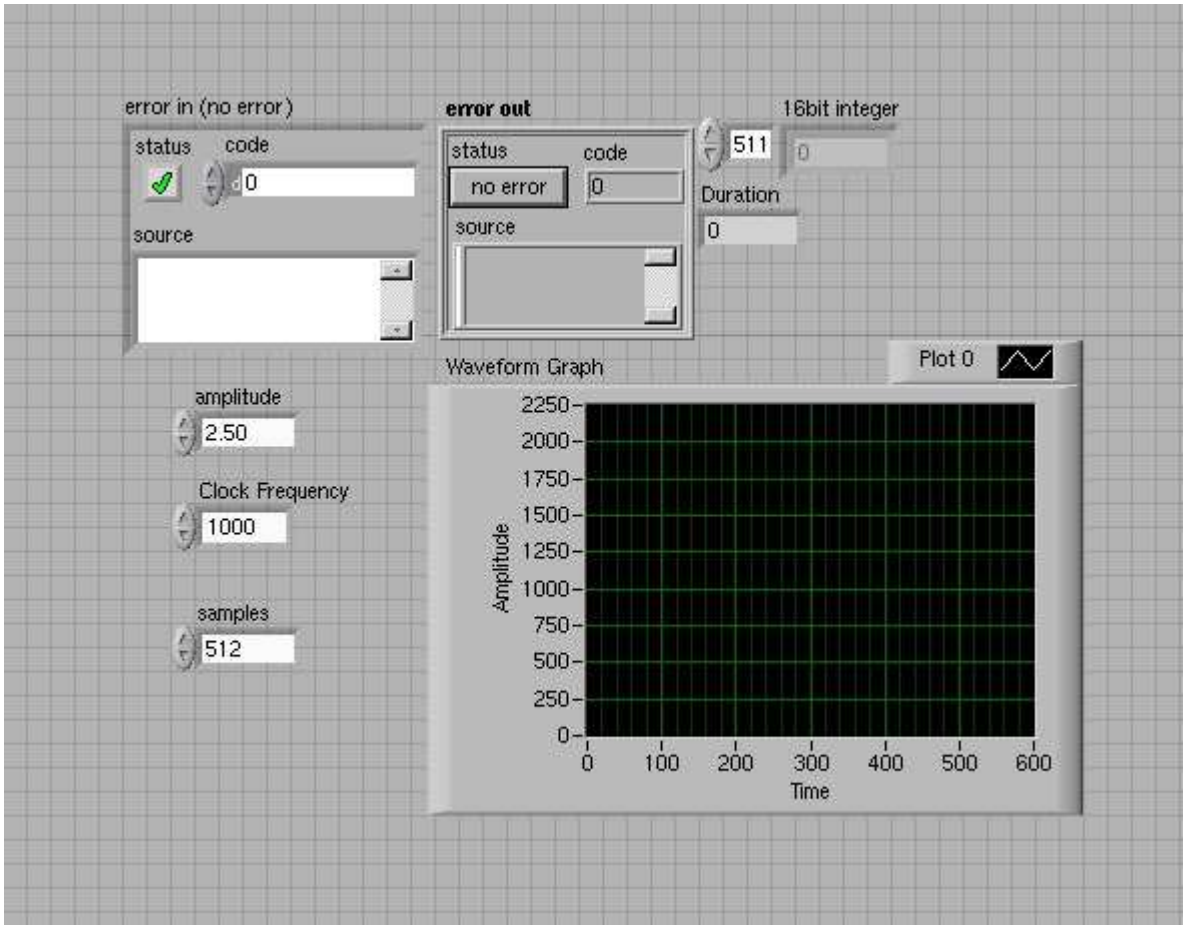

Figure A.7 Front Panel for Drop Seg Rings.vi. This VI writes one half of a sinusoidal signal to the CAMAC crate that we use to control the drop of the segmented rings.

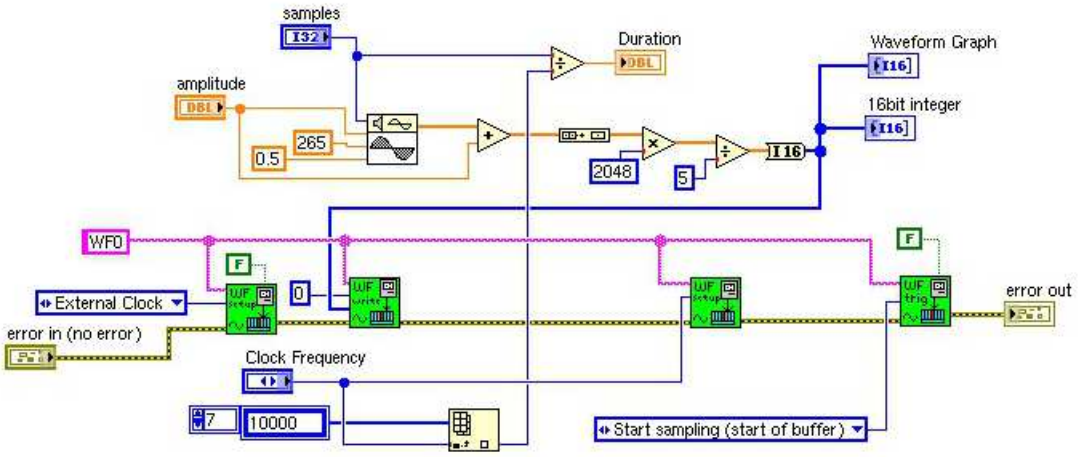

Figure A.8 Block Diagram for Drop Seg Rings.vi. This VI writes one half of a sinusoidal signal to the CAMAC crate that we use to control the drop of the segmented rings.

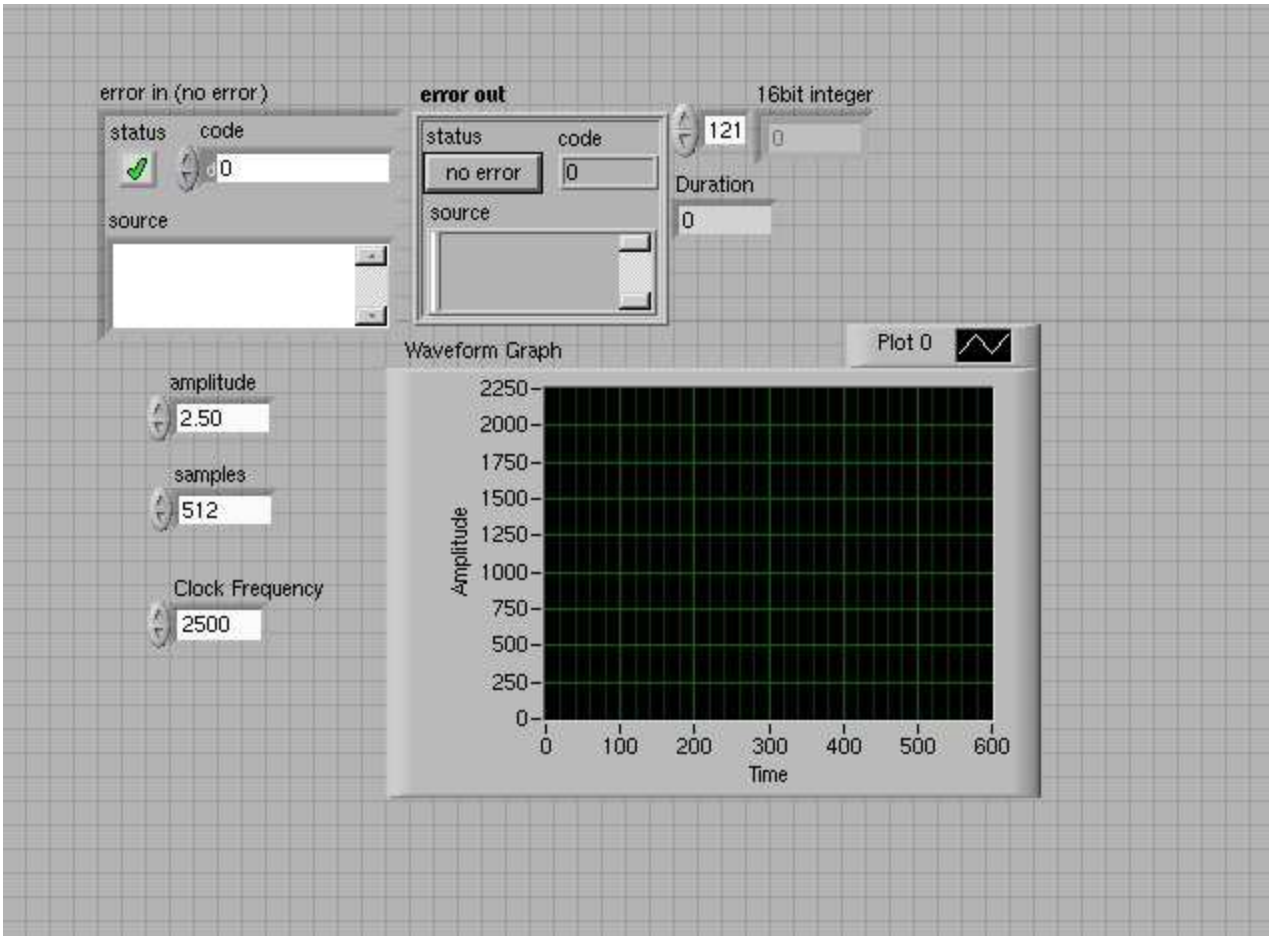

Figure A.9 Front Panel for Raise Seg Rings.vi. This VI writes one half of a sinusoidal signal to the CAMAC crate that we use to control the rise of the segmented rings.

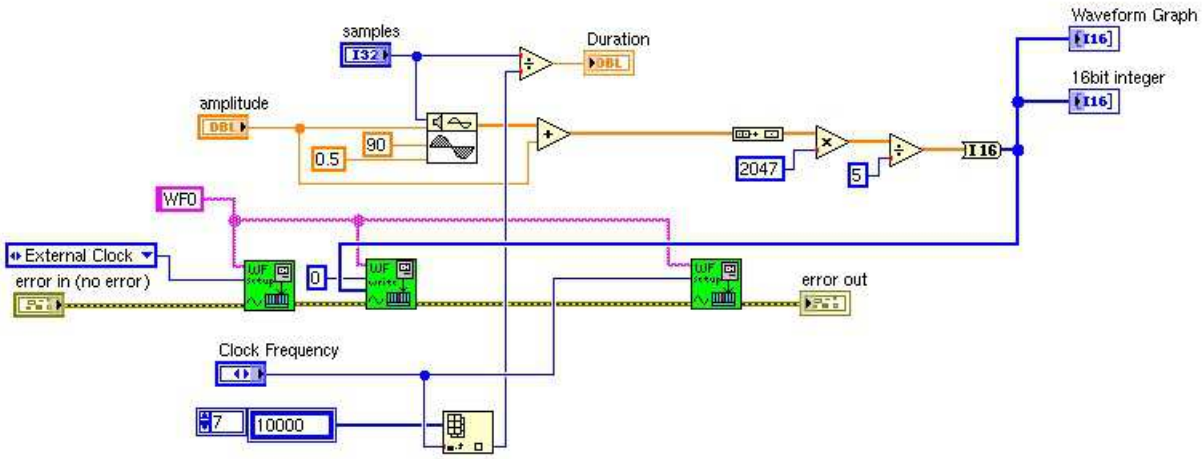

Figure A.10 Block Diagram for Raise Seg Rings.vi. This VI writes one half of a sinusoidal signal to the CAMAC crate that we use to control the rise of the segmented rings.

Bibliography

[1] C. Papastefanou and A. Ioannidou, "Beryllium-7 and solar activity," Appl. Radiat. Isot. 61 (2004).

[2] A. Ioannidou and C. Papastefanou, "Atmospheric beryllium-7 concentrations and sun spots," Nucl. Geophys. **8,** 539–543 (1994).

[3] S. A. Fitzgerald, J. V. Klump, P. W. Swarzenski, R. A. Mackenzie, and K. D. Richards, "Beryllium-7 as a tracer of short-term sediment deposition and resuspension in the Fox River, Wisconsin," Environ. Sci. Technol. **35,** 300–305 (2001).

[4] J. N. Bahcall, in *Neutrino Astrophysics* (Cambridge University Press, 1989), pp. 63–67.

[5] C.-A. Huh, "Dependence of the decay rate of ^{7}Be on chemical forms," Earth Planet. Sci. Lett. **171,** 325–328 (1999).

[6] P. Voytas *et al.*, "Direct measurement of the L/K ratio in ^{7}Be electron capture," Phys. Rev. Lett. 88 (2002).

[7] P. Das and A. Ray, "Terrestiral ^{7}Be decay rate and ^{8}B solar neutrino flux," Phys. Rev. C 71 (2005).

[8] H. Johlige, D. Aumann, and H.-. Born, "Determination of the relative electron density at the Be nucleus in different chemical combinations, measured as changes in the electron-capture half-life of ^{7}Be," Phys. Rev. C 2 (1970).

[9] Z. Liu, C. Li, S. Wang, J. Zhou, Q. Meng, S. Lu, and S. Zhou, "Measurement of change of ^{7}Be decay rate in Be and Au," Chin. Phys. Lett. 20 (2003).

[10] E. Norman, G. Rech, E. Browne, R.-M. Larimer, M. Dragowsky, Y. Chad, M. Isaac, R. McDonald, and A. Smith, "Influence of physical and chemical environments on the decay rates of ^{7}Be and ^{40}K," Physics Letters B **519,** 15–22 (2001).

[11] F. Lagoutine, J. Legrand, and C. Bac, "Half-lives of some radionuclides," Int. J. Appl. Radiat. Isot. **26,** 131–135 (1975).

[12] M. Maeger, S. Wilmes, V. Kölle, and G. Staudt, "Precision mesurement of the half-life of ^{7}Be," Phys. Rev. C 54 (1996).

[13] A. Ray, P. Das, S. Saha, S. Das, B. Sethi, A. Mookerjee, C. B. Chaudhuri, and G. Pari, "Observation of large change of ^{7}Be decay rate in Au and Al_2O_3 and its implications," Physics Letters B **455,** 69–76 (1999).

[14] X.-P. Huang, F. Anderegg, E. M. Hollmann, C. F. Driscoll, and T. M. O'Neil, "Steady-State Confinement of Non-neutral Plasmas by Rotating Electric Fields," Physical Review Letters 78 (1997).

[15] J. R. Danielson and C. M. Surko, "Radial compression and torque-balanced steady states of single-component plasmas in Penning-Malmberg traps," Phys. Plasma 13 (2006).

Index